

Brillouin Spectra of Porous p-Type 6H-SiC

G. T. Andrews^{1,a}, C. Young^{1,b}, A. Polomska^{1,c}, M. J. Clouter^{1,d},
Y. Ke^{2,e}, R. P. Devaty^{2,f} and W. J. Choyke^{2,g}

¹Department of Physics, Memorial University, St. John's, Newfoundland A1B3X7, Canada

²Department of Physics & Astronomy, University of Pittsburgh, Pittsburgh, PA 15260, USA

^atandrews@physics.mun.ca, ^bcyoung@physics.mun.ca, ^cannap@physics.mun.ca,
^dclouter@physics.mun.ca, ^eyuk4@pitt.edu, ^fdevaty@pitt.edu, ^gchoyke@pitt.edu

Keywords : Porous SiC, Brillouin scattering, surface acoustic waves, elastic properties

Abstract. Brillouin spectra have been recorded for a series of supported films of p-type porous 6H-SiC with a branched morphology and porosities in the range from 30% to 58%. Complex spectra comprising up to 7 identifiable components were observed in some cases. An effective medium model is being developed as an aid in interpreting the spectra, and preliminary results are presented.

Introduction

The thermally excited surface acoustic waves (SAWs) that are probed by the Brillouin scattering process have a wavelength of the same order as the optical wavelength and extend only a wavelength or two into the medium. They are consequently well suited for probing the properties of etched or epitaxial layers with comparable thicknesses. While there are several possible surface modes, the most commonly observed mode is the Rayleigh wave, which is characterized by displacements that are predominantly normal to the unperturbed surface. For these waves in the particular case of back scattering employed here, the frequency shift (in Hz) is given by $\nu = (2V_{\text{SAW}}/\lambda)\sin\theta$ where V_{SAW} is the SAW velocity, θ is the angle of incidence of the laser beam (relative to the surface normal), and λ is the wavelength of the incident light. This angular dependence is the identifying signature of the SAW modes.

Experimental Setup and Sample Details

A typical back-scattering geometry is shown schematically in Fig. 1. The laser with a stable line width of ~ 10 MHz or less at $\lambda=532$ nm was directed by a small prism through the focussing lens, L, on to the sample, S. The beam was polarized in the plane of incidence with a power of ~ 40 mW. When considered appropriate the sample was enclosed in an evacuable chamber, C, which was fitted with a thin glass window, W. The chamber was rotatable about the normal to the diagram so that the angle of incidence (θ) of the beam on to the sample surface could be varied. The light scattered backward along the incident laser-beam was collimated by the lens, L, and directed to the tandem Fabry-Perot interferometer (FP).

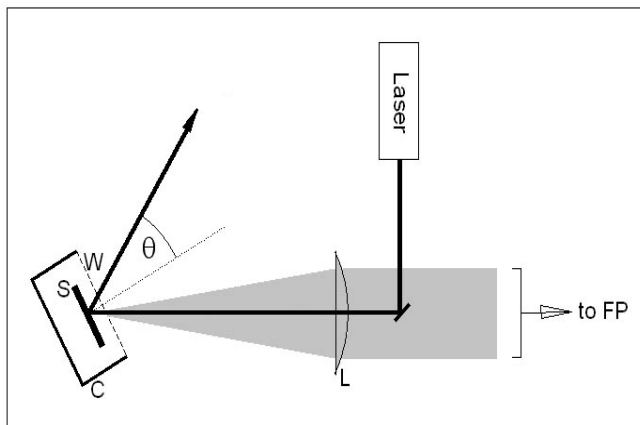


Figure 1. Scattering geometry

The light scattered backward along the incident laser-beam was collimated by the lens, L, and directed to the tandem Fabry-Perot interferometer (FP).

For optically transparent materials such as SiC the SAW modes are often difficult to detect. However, a light coating of Al with a thickness of 20 to 50 nm is often sufficient to overcome this problem. If necessary, an extrapolation to zero coating thickness will reveal the true SAW velocity on the (free) surface of interest. All Al-coated samples

were maintained in a low humidity environment at all times.

The porous samples were produced by etching the (0001) carbon face of p-type 6H-SiC crystals (carrier concentration approximately $7 \times 10^{18} \text{ cm}^{-3}$) using an aqueous electrolytic solution containing 10% HF and 5% ethanol. The normals to the etched surfaces were all tilted at 3.2° off the [0001] direction towards $[11\bar{2}0]$.

The current densities and times employed varied from 2 to 32 mA/cm^2 and 0.75 to 6 hours, respectively. The samples were not exposed to UV radiation during the etching process. The resulting 6 samples that were examined had gravimetrically determined porosities of 30%, 35%, 39%, 56%, 57%, and 58% with an average thickness of $27 \mu\text{m}$. Scanning electron microscopy revealed the morphology to be of the *branched (algae)* type [1].

Experimental Results

The first sample investigated was coated with 40 nm of Al and had a porosity of 56%. A series of spectra of this sample is shown in Fig. 2. Although the angular variation of the two peaks near 10 GHz is suggestive of SAW behavior, linear fits to the shift data did not extrapolate through $\sin\theta = 0$ for either of these two features. This criterion is better satisfied by the sharper of the two features which indicates a velocity in the range from 3800 to 3900 m/s. The spectra of other Al-coated samples were generally more complicated with up to 5 identifiable features being present.

The sample of 56% porosity was selected for further investigation with the intent of applying Al coatings of different thickness as a means of assessing any effects associated with the coating. The initial coating was removed by immersion in a 50% aqueous solution of HCl for several hours. It turned out, rather surprisingly, that a spectrum could be obtained from the uncoated sample. This spectrum is shown in Fig. 3 where the mirrored left half of the spectrum has been omitted in order to better show the details. For clarity a very intense ghost of the $\nu=0$ line (which is a characteristic of the tandem instrument) has also been omitted between 100 and 120 GHz. The peak **a** was verified to be due to the sample holder and should be ignored. The sharp peaks **e**, **f**, and **g** are identified as bulk modes of the non-porous crystal substrate [2] and the broad peaks **b**, **c**,

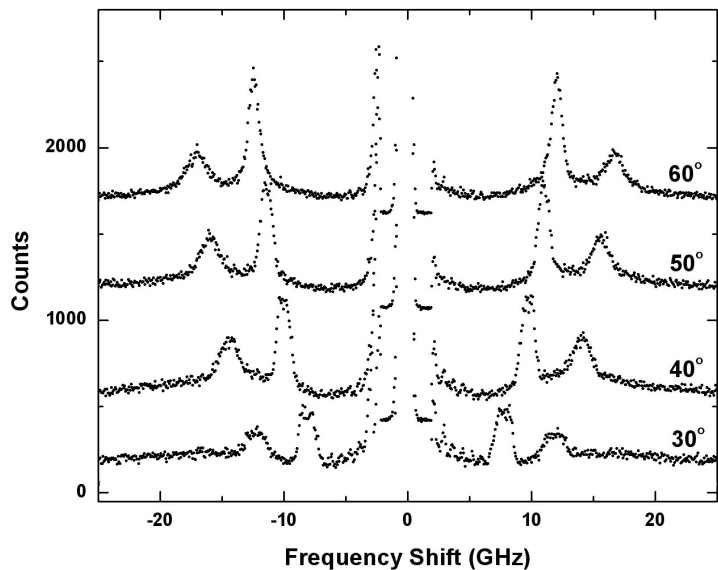


Figure 2. Brillouin spectra of Al-coated 56% porous 6H-SiC for a series of incident angles (θ).

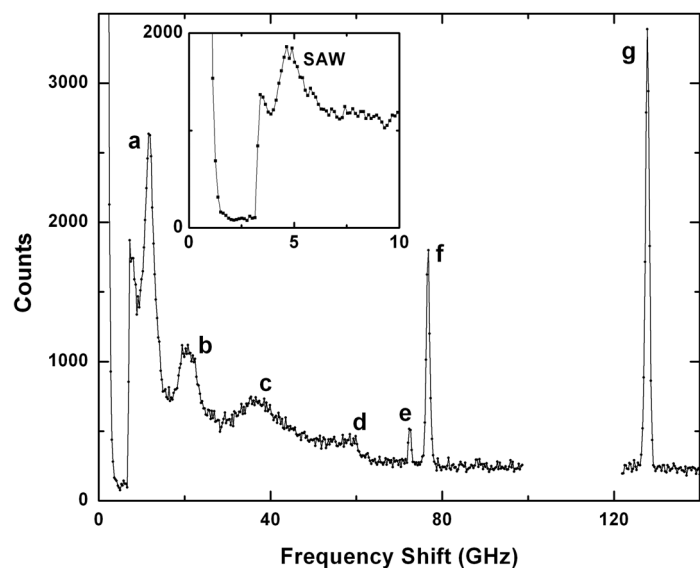


Figure 3. Brillouin spectrum of uncoated 56% porous 6H-SiC at an incident angle of 50° .

and **d** at 20 GHz, 37 GHz, and 60 GHz, respectively, are tentatively assigned as bulk modes of the porous film which are expected to be highly attenuated. All 6 of these peaks show only small changes in shift with varying angle of incidence. There is no SAW component discernible in the main body of Fig. 3 but it is shown as an inset which is extracted from a higher resolution spectrum. The $\sin\theta$ dependence of the shift in this case is unambiguous (see Fig. 4) and yields a SAW velocity of 2820 ± 70 m/s.

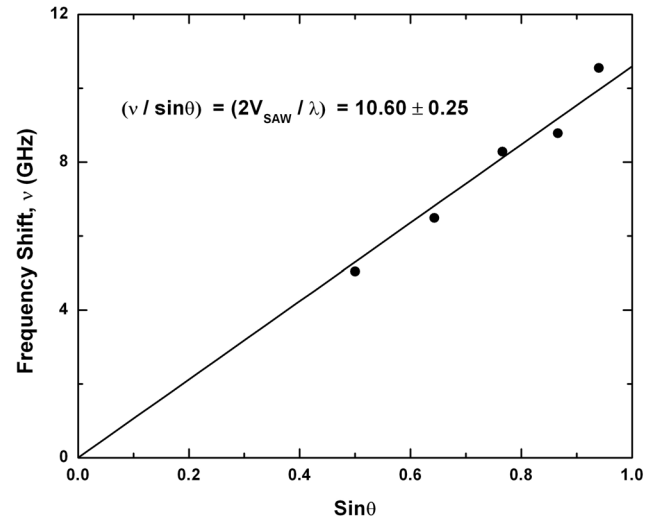


Figure 4. Linear fit to v versus $\sin\theta$ for the SAW peak.

Effective Medium Model and Discussion

The effective medium approximation is applicable when the wavelength exceeds the characteristic size of the inclusions in a heterogeneous medium. Here the inclusions are pores in the single crystal 6H-SiC host. The complex microstructure of porous 6H-SiC is replaced by a homogeneous medium characterized by effective elastic constants. We use the effective elastic constants to calculate the porosity dependence of the SAW speed of the Rayleigh wave and compare the results to the measurements.

The challenge is to calculate the acoustic properties of a uniaxial crystal permeated with a complex morphology of pores. The most general case that can be treated analytically allows inclusions that are ellipsoids of revolution with symmetry axes parallel to the crystal c -axis. The generalized Eshelby tensor is required to account for the boundary condition between inclusion and host, including the effects of the shape of the inclusion. Very recently, this tensor has been calculated analytically for the case of an ellipsoidal inclusion in a transverse isotropic elastic medium [3-4]. The calculation makes use of a special tensor basis based on the symmetry. We cannot present the details of the calculation here due to the limitations in length, but will do so in a future publication.

There are many choices available for the effective medium. Two examples for elastic waves are the Mori-Tanaka model and the self-consistent model [5]. In the Mori-Tanaka model, the calculated effective elastic constants are nonzero over the complete range of porosities. When applied to an elastic medium with spherical pores, the self-consistent model predicts that the effective elastic constants vanish for porosities above 50%. Clearly, such behavior does not provide a good representation of our data. Therefore, we choose the Mori-Tanaka model.

The input data for the calculation are the porosity, the elastic constants of crystalline 6H-SiC, and the shape factor $\xi = a/a_3$, where $a_1 = a_2 = a$ and a_3 are the semimajor axes of the ellipsoidal inclusions, which are ellipsoids of revolution coaxial with the crystal c -axis. We use the elastic constants of 6H-SiC measured by Kamitani et al. [2] using Brillouin scattering: $C_{11} = 501$, $C_{33} = 553$, $C_{44} = 163$, $C_{12} = 111$ and $C_{13} = 52$ GPa. The Rayleigh SAW speed is calculated for waves propagating on a basal surface [6]. For this initial calculation, we neglect piezoelectric coupling and impose zero stress boundary conditions at the surface. The derivation leads to a cubic equation for the square of the SAW speed. We choose the single root which leads to a real decay constant, corresponding to a wave localized at the surface, for the case of bulk (nonporous) SiC.

Fig. 5 shows the calculated SAW speed for spheres, prolate spheroids and oblate spheroids. The curves for prolate spheroids and spheres are nearly identical, but the former is slightly higher than the latter. Oblate spheroids lead to a substantial reduction of the SAW speed. Although the calculated morphology of ellipsoidal inclusions is certainly not an accurate

representation of the branched morphology, it is worth noting that the Mori-Tanaka model with oblate spheroids of shape factor $\xi = 5$ provides a calculated SAW speed of 2841 m/s at 56% porosity, in good agreement with the measured speed of 2820 ± 70 m/s.

Conclusion

Our success in observing surface and bulk acoustic waves in porous p-type 6H-SiC, and in applying relatively simple models to gain insight into the observed behavior, encourages us to pursue this work along several lines. The model demonstrates the importance of morphology in determining the behavior of acoustic waves in a porous material, suggesting further Brillouin scattering measurements on a variety of the morphologies of porous SiC that we have produced. The next step in the modeling is to include the effects of piezoelectricity.

Acknowledgements

The Memorial University group wishes to acknowledge the assistance of Mr. Robert Boyd in the collection and analysis of data, and also the financial support provided by the Natural Sciences and Engineering Council of Canada. The University of Pittsburgh group thanks the DURINT program (ONR N00014-01-1-0715) for support of this research.

References

- [1] Y. Shishkin, Y. Ke, R.P. Devaty and W.J. Choyke: *J. Appl. Phys.* 97 (2005), 044908.
- [2] K. Kamitani, M. Grimsditch, J.C. Nipko, C.-K. Loong, M. Okada, and I. Kimura: *J. Appl. Phys.* 82 (1997), p. 3152.
- [3] V.M. Levin and M.G. Markov: *Int. J. Solids Struct.* 42 (2005), p. 393.
- [4] I. Sevostianov, N. Yilmaz, V. Kushch and V. Levin: *Int. J. Solids Struct.* 42 (2005), p. 455.
- [5] S. Torquato: *Random Heterogeneous Materials* (Springer, New York 2002).
- [6] C.-C. Tseng and R.M. White: *J. Appl. Phys.* 38 (1967), p. 4274.

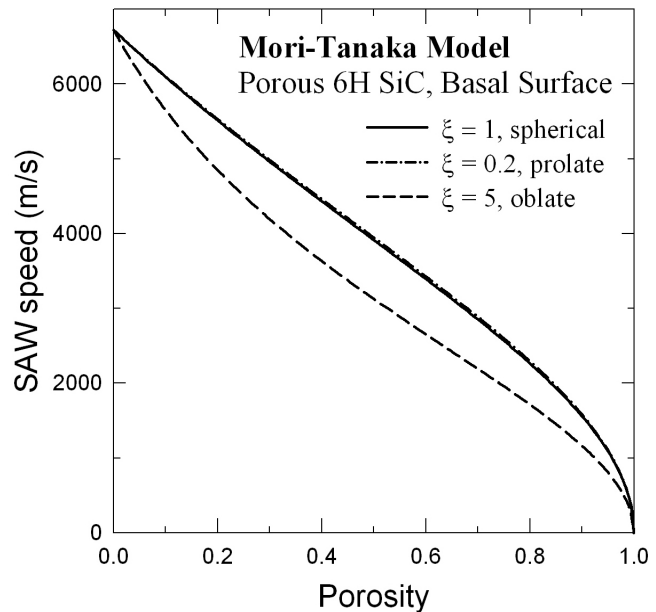


Figure 5. Calculated Rayleigh SAW speed in porous 6H-SiC. The parameter $\xi = a/a_3$ specifies the shape of the ellipsoidal pores.